KMS Technologies – KJT Enterprises Inc.

Chapter 3
Distortions of the Signal and their Compensation

extract from

Strack, K.-M., 1992**,** reprinted 1999
Exploration with deep transient electromagnetic: Elsevier, 373 pp.

Chapter 3
Distortions of the Signal and their Compensation

After considering the physical background of deep transient electromagnetics, one needs to be aware of possible problems encountered when measuring, processing and interpreting real field data. These problems can be overcome by either carefully correcting for them or by avoiding them as much as possible. For better evaluation and selection of the tools required, the possible errors are categorized in three classes.

- Errors caused by the choice of the hardware system such as transmitter input waveform and receiver filters.
- Errors caused by external anthropogenic influence introducing electromagnetic noise into the signal recorded.
- Errors caused by the local geology such as unknown near-surface lateral resistivity variations.

In this chapter, possible solutions are given for the above errors. One way of correction for the transmitter input waveform and receiver system filters is a careful consideration of the system response. After measuring this response, one can deconvolve it from the data. Anthropogenic (man made) electromagnetic noise can be removed using digital signal processing techniques. The digital processing of the field data is the area where most of the signal-to-noise improvements can be obtained. This is emphasized in this chapter. Distortions caused by 3-D geology are not considered in this section because these signals are the wanted information. Most of the typical distortions are from near-surface lateral resistivity inhomogeneities which cause transmitter overprints. Using some insight into the physical behavior of electromagnetic fields, most of these can be corrected in the magnetic field measurements.

Only the combination of all techniques and careful evaluation of the data behavior guaranties that LOTEM can be applied in most environments. In very noisy environments one often has to apply the filters prestack to get optimum signal-to-noise ratios.

THE FIELD PROBLEM

During field data acquisition, the output signal consists of the input signal combined somehow with the effects of the entire data generation process. This can be

visualized through the *Black Box* concept with the *true signal*, the earth response, going into a *Black Box* where it is modified. The output is the measured signal. In the field, the *Black Box* is a combination of distortions in the data acquisition and transmitter systems. The transmitter system introduces distortions due to imperfections in the transmitter waveform and coupling effects (induced polarization etc.) with the subsurface. The data acquisition system introduces distortions from the receiver side (amplitude response, temperature drifts, receiver misorientation, etc.).

Fig. 3.1: *Black Box* concept for the signal path.

Mathematically, the *Black Box* concept can be described as convolution of

$$\text{Input}(t) * \text{Black Box}(t) = \text{Output}(t) \tag{3.1}$$

or

$$\text{Output}(t) = \int_{-\infty}^{\infty} \text{Input}(t-\tau)\ \text{Black Box}(\tau)\ d\tau. \tag{3.2}$$

The *convolution* process can be performed by taking the time series *Input* and *Black Box*, reversing *Black Box* and performing a serial multiplication of *Input* with the reversed *Black Box* (Bracewell, 1978). The effect of the systematic distortion of the signal can be removed from the measured earth response by using the inverse of the *convolution* called deconvolution, which will be described later on.

In addition to the transformation by the earth and the recording system, different sources of noise are superimposed on the signal. Whereas above system distortions are convolutions, this noise is added to the signal as shown in figure 3.2.

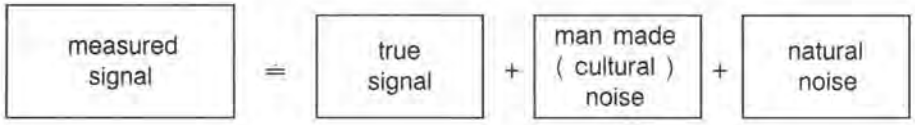

Fig. 3.2: Combination of noise sources with the true signal.

Noise can be classified into *periodic* and *sporadic noise*. *Periodic noise* can be removed with digital filters and sporadic noise by using selective stacking techniques.

Periodic noise is mainly generated by power lines, telephone lines and the power consumers. *Sporadic noise* is caused by current surges in the power network, machinery, motion of magnetic material near the receiver and external magnetic field variations. Natural noise caused by ionospheric currents and geologic structures can severely distort the signal. In most instances it will be unrecoverable unless special natural noise compensation techniques are used. To date, one way of overcoming the natural noise is to increase the transmitter moment to a level where the signal can be measured with the field system. Other ways of overcoming the noise are for frequency domain EM systems remote referencing (Clarke et al, 1983), or pseudo random binary sequence (PRBS) systems which use encoded signals (Duncan et al, 1980). For LOTEM field applications we found a transmitter moment increase or local noise compensation (LNC) (Stephan and Strack, 1991) work best to overcome the noise problem. New multichannel systems integrating field procedures, newest data processing principles and state-of-the-art electronics can further improve the signal-to-noise ratios.

At this stage, the reader is referred to some classic papers and textbooks (Shanks, 1967; Kulhanek, 1976) for the derivation of the digital recursive filters. In this chapter, only the results necessary for understanding the LOTEM data processing and filtering are included.

DECONVOLUTION OF THE SYSTEM RESPONSE

The ideal theoretical response of a polarity reversing transmitter at the receiver is influenced by the following effects:

- Deviation of the current waveform from a step (ramp) function.
- Off-time between the polarity reversals.
- Polarization effects near the electrodes and sensors.
- Inductance of transmitter wire.
- Near-surface lateral resistivity inhomogeneities.
- Misalignment of the receiver.
- Frequency response of the receiver.
- Analog electronics of the amplifier and preamplifier (notch filters).
- A/D converter temperature drift.

All of these yield the *true* system response when convolved with each other. They must be eliminated from the measured signal in order to obtain the *true* signal. Using conventional digital signal processing principles would mean that one can measure the system response accurately, when inputting a spike (delta function) and measuring the output. Since a delta function in practice can not be realized as input, a square wave is input and the derivative of the output is calculated. Three of the items in the above list cannot be included into the system response measurements, namely near-surface lateral resistivity variations, the misalignment errors of the receiver, and the temperature

drift of the A/D converter. We assume that the temperature drifts of the state-of-the-art A/D converter are small and are statistically included by measuring the system response many times and then averaging it. The receiver misalignment and lateral inhomogeneities can give us a static shift of the signal, which is removed from the magnetic field using the MMR correction or calibration factor (see below). The remaining system influence is measured by using the switchbox to generate the square wave which is then input into the data acquisition system.

Rewriting the input/output equation 3.1 with x(t) being the *input*, y(t) the *output*, and s(t) the *Black Box*, we obtain:

$$y(t) = s(t) * x(t) \tag{3.3}$$

The deconvolution of the *system response* s(t) (the *Black Box*) can be done in three different ways:

First, using the convolution theorem (Bracewell, 1978), the above equation can be transformed to the frequency or z-domain yielding a simple multiplication:

$$Y(z) = S(z) * X(z) \tag{3.4}$$

If we divide Y(z) by S(z) we obtain X(z). For transient data this procedure becomes very difficult, since the frequency content of the system response is too similar to the frequency content of the transient signal. Also, the frequency spectrum of the signal and the system response contains holes in them when analog notch filters have been used during data recording. Calculation of the inverse of S(z) thus can cause instabilities due to the inverse of numbers close to zero. To date, nobody has successfully implemented the above method for transient data (Bond et al, 1981; Strack, 1981; Rossow, 1987). This principal problem can also be understood by using the time-frequency equivalent. The transient system response is designed to be as narrow as possible in time domain, in order to have the least influence on the signal. Narrow in time, however, means broad in frequency which is why frequency deconvolution will always increase the noise on the signal.

Second, one can use a deconvolution scheme in time domain similar to the one in the frequency domain, but using numerically stable procedures. This convolution scheme was developed by Stoyer in 1981 (Stoyer and Strack, 1984; Strack 1985), and although specifically developed for transient data, it is very similar to the one developed by LaCoste (1982) and Ioup and Ioup (1983). The algorithm is based on the van Citert iteration:

$$\begin{aligned} A_0 &= y(t) \\ A_1 &= A_0 + (y(t) - A_0 * s(t)) \\ &\cdots \\ &\cdots \\ A_m &= A_{m-1} + (y(t) - A_{m-1} * s(t)) \end{aligned} \tag{3.5}$$

It can be shown that, if m goes to infinity, A_m approaches x(t) (see proof in appendix 1). When doing the above deconvolution, the convergence to x(t) is often reached after 3 to 5 iterations. A side effect of this type of deconvolution is the signal-to-noise ratio improvement, whereas the frequency domain deconvolution amplifies the noise. Figure 3.3 shows an example of a signal with and without the time domain deconvolution.

The left side of the figure shows the data set after deconvolution in a linear stacked data display and as early and late time apparent resistivities. Note the amplitude recovery at early times in comparison to the stacked data on the right side of the figure. The flair up of the 95% confidence level in the early time apparent resistivity curves is caused by the noise around the onset (first data point after the t=0 vertical marker line) which often brings this data point below the zero level causing stability errors in the logarithmic display.

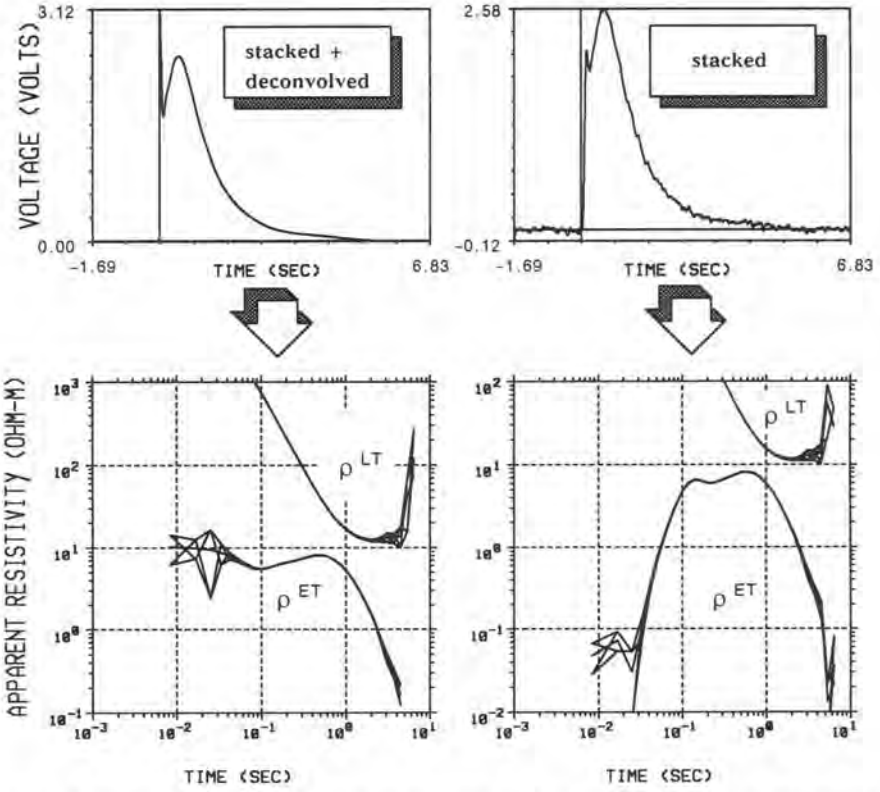

Fig. 3.3: Example of a selectively stacked transients with (left) and without (right) time domain deconvolution of the system response.

Third, one can replace the deconvolution in the data processing sequence by a convolution of the synthetic data with the system response in the inversion/for-

ward modeling phase. This must be done when the length of the system response is more than one third of the length of the transient (rule of thumb). We recommend that this and the second method be carried out for each survey and the best (most stable) and fastest way selected.

RECURSIVE DIGITAL FILTERS

Since we know how to remove distortions due to systematic errors in our own system, we can now consider the distortions due to external influences. One kind of distortion is caused by periodic noise, which can not be completely filtered out using analog filters. However, it can be significantly reduced using digital recursive filters. Following is a description of the *true amplitude recursive filters* (Strack et al, 1988).

In general, one can divide linear digital filters in two categories: a non-recursive and a recursive filter. The non-recursive filter only uses the input data to get the output whereas a recursive filter uses previously output data to evaluate the present output. More easily this is seen in the difference equation:

$$y(n) = \sum_{k=1}^{M} a_k y(n-k) + \sum_{k=0}^{N} b_k x(n-k), \tag{3.6}$$

If all $a_k \equiv 0$, we have a non-recursive filter, whereas if $a_k \not\equiv 0$ the filter is recursive. The values M or N denote the order of the filter.

Since we are interested in filtering out periodic noise, we construct a recursive second order notch filter which is true in amplitude and phase and has a small bandwidth. The following shows the derivation of a phase and amplitude preserving digital recursive filter using the z - transform. The z - transform can be considered as a generalization of the Fourier transform for discrete time series x(n) which is the discrete representation of the function x(t). The z - transform of x(n) is given by

$$X(z) = \sum_{n=-\infty}^{\infty} x(n) z^{n} \quad ; \quad z \in \mathbb{C} \tag{3.7}$$

$$\text{with} \qquad z = r e^{-i\omega} \tag{3.8}$$

where r is the radius vector in the z-plane.

The z - transform can be interpreted as the Fourier transform of x(n) multiplied by an exponential sequence. For r = 1, (i.e. $|z| = 1$), the z - transform of x(n) is equal to the Fourier transform of x(n).

The convolution theorem is used for the construction of a filter by taking the difference equation and performing a z-transform, giving:

$$Y(z) = \sum_{k=1}^{M} a_k z^{k} Y(z) + \sum_{k=0}^{N} b_k z^{k} X(z), \tag{3.9}$$

With this form of the difference equation we get the relationship between the filter coefficients and the filter response function:

$$H(z) = \frac{Y(z)}{X(z)} = \frac{\sum_{k=0}^{N} b_k z^k}{\left(1 - \sum_{k=1}^{M} a_k z^k\right)} \qquad (3.10)$$

The frequency response of the above H(z) can be evaluated on the unit circle where $|z| = 1$. We choose (1,0) to be 0 frequency and (−1,0) to be the Nyquist frequency, f_N.

Since H(z) is a rational function we must consider poles and zeroes of H(z) which are the values where H(z) is infinite and zero, respectively. With a notch filter in mind we want the frequency response of H(z) to be 0 at the notch frequency f_o. This means that a zero of H(z) is located at $z_n = (\cos\phi, \sin\phi)$. This is done by choosing the a_k and b_k such that $H(z_n) = 0$. A filter with small bandwidth is obtained by placing a pole right next to the zero z_n, which assures us that H(z) is only zero for a small range around the notch frequency f_o. The nearer the pole z_p and the zero z_n, the smaller is the bandwidth of the filter.

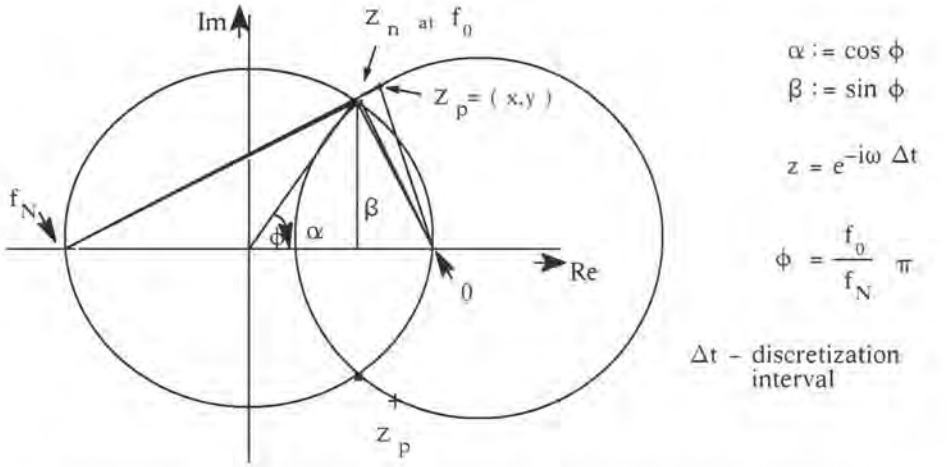

Fig. 3.4: Schematic of the pole–zero technique in the complex plane for the construction of a digital recursive filter.

However, since the amplitude and shape of the transient contains most of the resistivity information, it is essential that the digital filter should not only suppress the noise but maintain the amplitude. This gives us a further condition for the placement of the poles and zeroes, since this can be only achieved when the pole is located on the Appollonian circle, which means that:

$$\frac{|z_n - 1|^2}{|z_n + 1|^2} = \frac{|z_p - 1|^2}{|z_p + 1|^2} \quad \text{or}$$

$$\frac{(1-\alpha)^2 + \beta^2}{(1+\alpha)^2 + \beta^2} = \frac{(1-x)^2 + y^2}{(1+x)^2 + y^2} \qquad (3.11)$$

In other words, the ratio between the vectors to the pole and zero will remain the same and yield a recursion formula in the z-plane.

$$H(z) = \frac{Y(z)}{X(z)} = \eta \frac{(z - z_n)(z - z_n^*)}{(z - z_p)(z - z_p^*)} = \eta \frac{z^2 - 2\alpha z + 1}{z^2 - 2\alpha\eta z + 2\eta - 1} \qquad (3.12)$$

$$\text{with} \quad \eta := \frac{z_p - 1}{z_n - 1} \qquad (3.13)$$

is the normalization for gain 1.

If we define $x := \eta\alpha$, we obtain (3.14)

$$y^2 = \frac{2x}{\alpha} - (1 - x^2) \qquad (3.15)$$

H (z) is the filter function given by the ratio of the output function Y (z), and the input function X (z); z_n and z_p are the positions of the zero and poles respectively; η is the proportionality factor which combines the real part of the pole x, with the real part of the zero α; η is also called the bandwidth, y is the imaginary part of the pole. To eliminate phase shifts, the recursive filter is applied twice to the data: first in the forward, and then in the reverse direction.

If we remember that multiplication with z means a shift by one step in the time domain, we obtain after simple reformulation of the above equations

$$Y_n = \frac{1}{(2n-1)} \left[\eta X_{n-2} \alpha \eta X_{n-1} + \eta X_{n-2} + 2 \alpha \eta Y_{n-1} - Y_{n-2} \right] \quad (3.16)$$

where

$Y_{-1} = Y_{-2} = X_0$ can be chosen as starting values.

In figures 3.5a–c, this recursive true amplitude notch filter has been applied to three different sets of synthetic data. For all curves in figures 3.5a–c, the superimposed, solid line is the noise-free synthetic input signal. The top curves in figures 3.5a–c show this synthetic signal plus 16 2/3 Hz periodic noise, which is characteristic of the German railroad power grid. The middle curves in figures 3.5a–c have been filtered with a bandwidth of $\eta = 1.02$, whereas the bottom curves have been filtered with a bandwidth of $\eta = 1.08$.

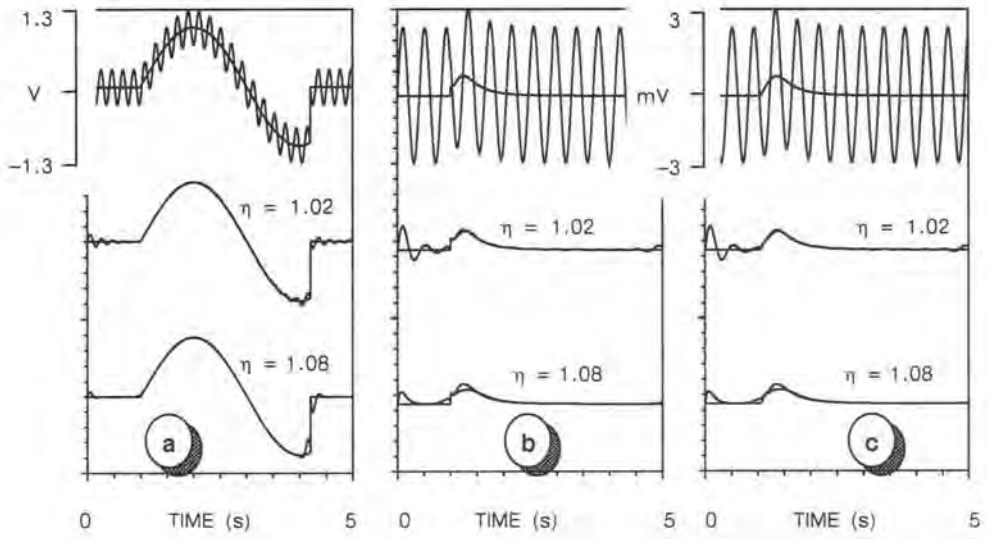

Fig. 3.5a–c: Example of a digital recursive notch filter applied to synthetic data. For all figures the noise – free synthetic input signal is superimposed for comparison. The bottom two curves are the results of applying the digital notch filter with different bandwidths to the top curve. For figure 3.5a, periodic 16 2/3 Hz noise is added to a sinusoid which abruptly starts, and ends with a step discontinuity. The synthetic curve in figure 3.5b represents an ideal theoretical transient. Figure 3.5c is the theoretical transient from figure 3.5b convolved with the impulse response of the recording system and transmitter, thus representing a real transient (after Strack et al, 1989).

In figure 3.5a, the synthetic signal is a sinusoid which abruptly starts and then ends with a step. The filtered curves show that due to the modest slope at the start of the sinusoid there are only minimal ringing effects. Ringing does occur at the step discon-

tinuity due to the Gibb's phenomenon. The ringing at the onset of the time series becomes less with increasing bandwidth and at the step, the ringing becomes greater with increasing filter bandwidth. In this example, there is almost no amplitude distortion.

The synthetic input signal of figure 3.5b represents an ideal transient where the signal rises instantaneously to its maximum. As with the step discontinuity in figure 3.5a, Gibb's phenomenon causes ringing at the onset of the transient. The filtered sinusoids also show the same correlation of bandwidth to ringing as those in figure 3.5a. Again, there is little or no amplitude distortion.

Figure 3.5c shows a realistic transient obtained from convolving the synthetic input curve of figure 3.5b with the impulse response of the receiver and the transmitter current waveform from our field system. The ringing due to filtering at the rise of the transient is much less than in figure 3.5b, since there is no longer a step discontinuity. For these data, there is almost no visible difference between the filtered signal and the input synthetic without noise. Since for $\eta = 1.08$, the filter introduces ringing at sharp edges (Gibb's phenomena), one usually tries to use the smallest η possible. At the same time this allows the filtering of a narrow frequency band.

The left side of figure 3.6 shows a typical single transient of average quality from a test area in Germany, contaminated by periodic 16 2/3 Hz railroad power grid noise. The right side of figure 3.6 shows the same transient after applying the digital notch filter. The signal information can now clearly be seen.

When this filter is applied prestack, there is almost no amplitude distortion and the periodic noise is filtered out. Since the 16 2/3 Hz noise, the 50 Hz noise, and their harmonics are not phase-correlated with the data acquisition, stacking smears the power line frequency and a digital notch filter applied poststack can not eliminate all the noise. Therefore, the filter must be applied before stacking.

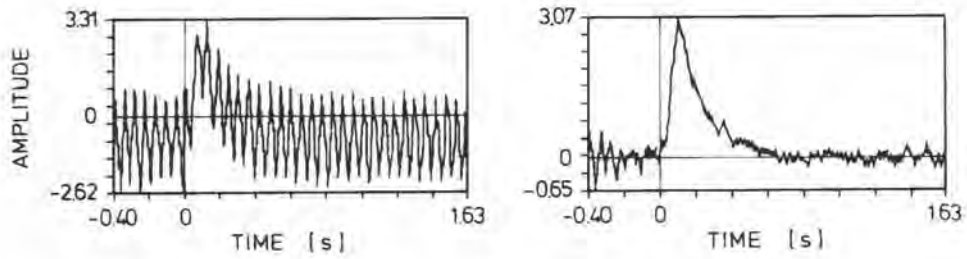

Fig. 3.6: Digital recursive, true amplitude notch filter applied to transient data. The left curve shows the original field data and the right curve the same data after filtering (after Strack et al, 1989).

One drawback of the digital recursive filters is the ringing when the transient rises sharply as can be seen in figure 3.5b. When using the new generation of acquisition hardware the signal is usually highly oversampled. Also, less analog filters are used

because of the high dynamic range. When in addition solid-state transmitters are used, the signal rises sharply (depending upon the subsurface resistivity) between the sample points. This gives significant problems because the above described recursive filters can, in some cases, ring so strongly that no transient can be recovered from the signal. In this case, a different filtering approach must be used. This approach is termed *lockin filter*, because it calculates from the data before the start of the transient the optimum periodic noise, locks to the phase of the noise and subtracts the noise from the single records prestack. The *lockin filter* consists of a series of sine and cosine functions which match the periodic component of the noise in a least squares sense. Figure 3.7 shows an example of a single record acquired with the TEAMEX multi-channel system which has a high dynamic range of 204 dB. The data were recorded

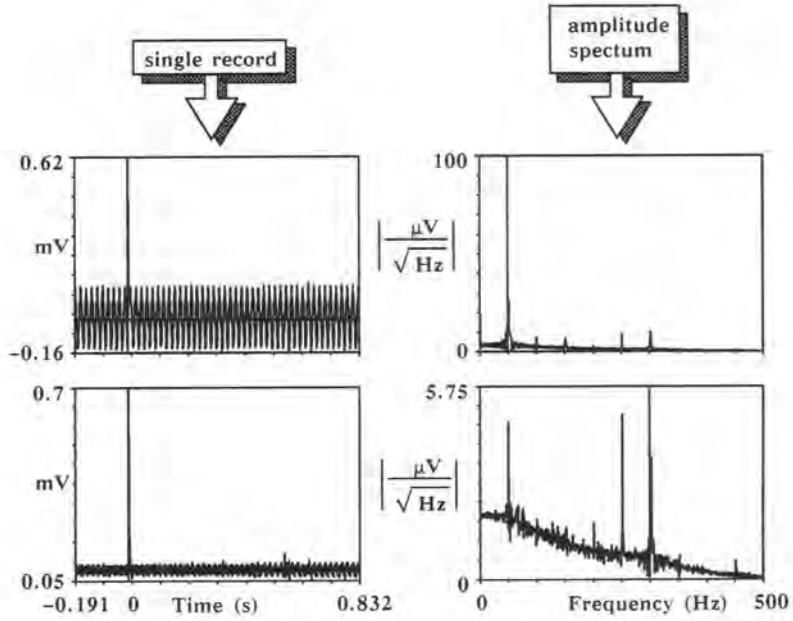

Fig 3.7: Example of a single transient contaminated with periodic noise. The left column shows the single record before and after filtering with a lockin digital filter. On the right side the respective amplitude responses are shown.

over highly resistive terrain in South Africa which explains the short length of a signal. On the left of the figure the single records are shown with the periodic noise (top) and after applying the digital *lockin filter* (bottom). Note that the noise has been reduced significantly. On the right side of the figure the respective amplitude responses are shown. Before filtering, the 50 Hz periodic noise is strongest with odd and even harmonics following. After applying the *lockin filter* the periodic noise up to 300 Hz has been significantly reduced (i.e. by approximately 20 times for 50 Hz). A very narrow signal was selected because it would be more distorted than a wider one. The narrow

signal is hardly effected by the *lockin filter* which would not be possible with a recursive filter. It should be emphasized that this filters should not be applied poststack because stacking smears the line characteristic of the noise.

SELECTIVE STACKING METHODS

Sporadic noise such as spikes may be caused by natural sources such as lightening and by many different cultural sources such as water pumps, electric fences, trains, factories and vehicles passing by the receiver. Once this noise is recorded and not recognized, it can severely distort the stacked results, since its amplitude is either far above or far below the average signal level (high or low energy spikes). When acquiring transients with a short rise time, it is also difficult to integrate a spike detector in either analog or digital form into the system, without the distorting of the transient itself.

A safe approach to eliminating this kind of noise is to consider the statistics of all signals and analyse their corresponding amplitude distributions, both of which become increasingly important when there are only a few transients and the sporadic noise is not canceled in the stacking process. Here we discuss two selective stacking techniques which use different rejection criteria to suppress sporadic noise: *symmetric* and the *area–defined rejection*. The symmetric selective stack, also known as alpha–trimmed mean (Watt and Bednar, 1983; Naess and Bruland, 1985), is less frequently used because of computational expense.

The first step in both selective stacking schemes is to sort the data amplitudes in ascending order for all transients at each time sample. Then for the symmetric rejection, a predetermined percentage of the total number of transients is symmetrically rejected from both ends of the sorted amplitudes. From the remaining percentage of data, a preliminary amplitude average and standard deviation are calculated (Stoyer, 1981). With the preliminary average and its standard deviation the sorted amplitude data set is reinspected and only data within a predetermined fraction of the standard deviation are kept. This procedure is very robust with respect to changes in the symmetric cutoff percentage which may be varied over a wide range (between 10 and 40%) where the low and high amplitude noise are removed.

For the area–defined rejection, amplitude frequency distributions are calculated by sliding overlapping windows over the sorted amplitude curves for each time sample of all transients. With this kind of rejection criteria, a percentage of the area under each distribution curve symmetric about the maximum is calculated, and all data within that area are kept.

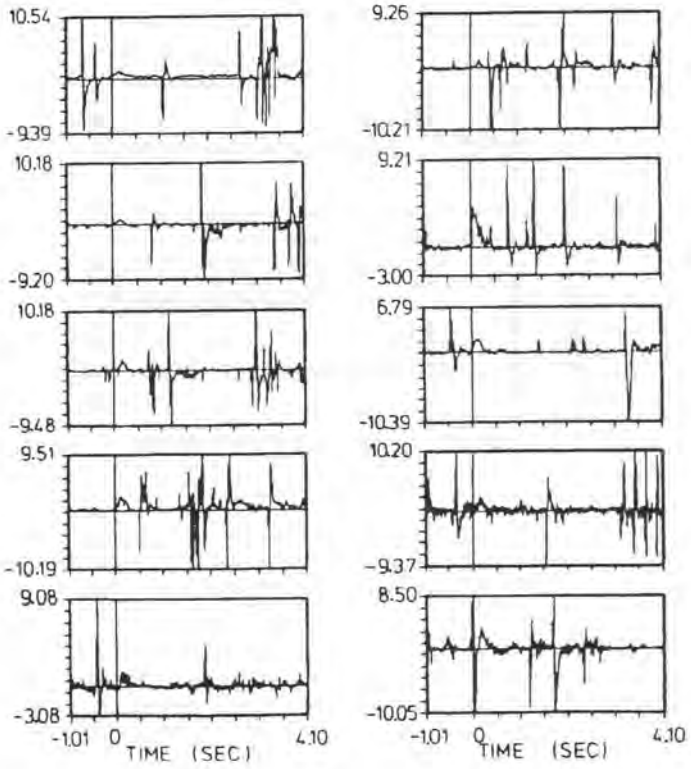

Fig. 3.8: Ten raw transients from Germany distorted by sporadic noise (after Strack et al, 1989).

An example of ten individual transients distorted by sporadic noise is given in figure 3.8. The elapsed time between the individual frames is approximately 20 seconds. Although the transient can be recognized directly after the vertical t=0 marker line, the predominant feature in the records are the spikes. These build parts of the data base (96 records) for the results shown in figures 3.9 through 3.11. The upper transient of figure 3.9 is the output of a straight average summation which did not cancel out the high and low energy noise. After calculating a preliminary amplitude average and standard deviation from all the field data, the data lying within two standard deviations of the average were then stacked. The lower transient of figure 3.8 is the result of this procedure. The high and low energy noise are now reduced and the signal-to-noise ratio improved.

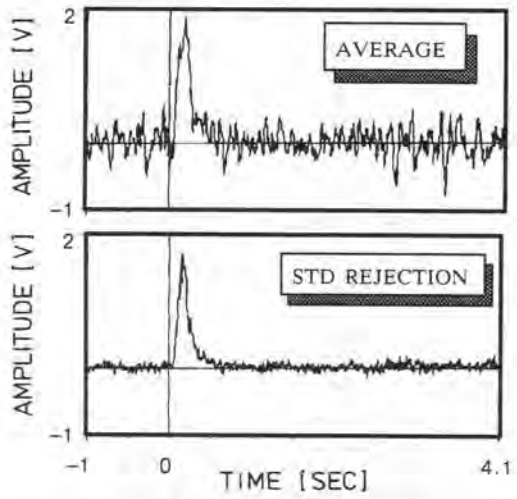

Fig. 3.9: Upper transient is the result of a straight average summation with poor signal–to–noise ratio.This stacking technique is improved by eliminating all amplitudes outside two standard deviations of the average ($-\sigma$, $+\sigma$) from the selective stack as shown in the lower transient (after Strack et al, 1989).

Figure 3.10 shows a selectively stacked transient based on the *symmetric rejection* criteria, using a 20% cutoff at both ends of the amplitude distribution. The frames at the right show two example amplitude distributions for different time samples. This transient displays an even higher signal–to–noise ratio than the transient shown at the bottom of figure 3.9. Similar results are obtained using the *area–defined rejection* selective stack with 60% of the area, as shown in figure 3.11. Amplitude frequency distribution curves are shown at the right where the shaded part of the curve is 60% of the kept area.

Figures 3.10 through 3.11 show that both the *symmetric rejection* and the *area–defined rejection* selective stack significantly improve the signal–to–noise ratio compared to the summation process which eliminated all data which lie outside of two standard deviations of the average (figure 3.9). This is because the average is already corrupted by the outlying sporadic noise amplitudes which, for the selective stacking schemes, are rejected before the average is calculated. For LOTEM soundings, our experience has been that the *symmetric rejection* stack gives us the best signal–to–noise ratios for the data from most survey areas.

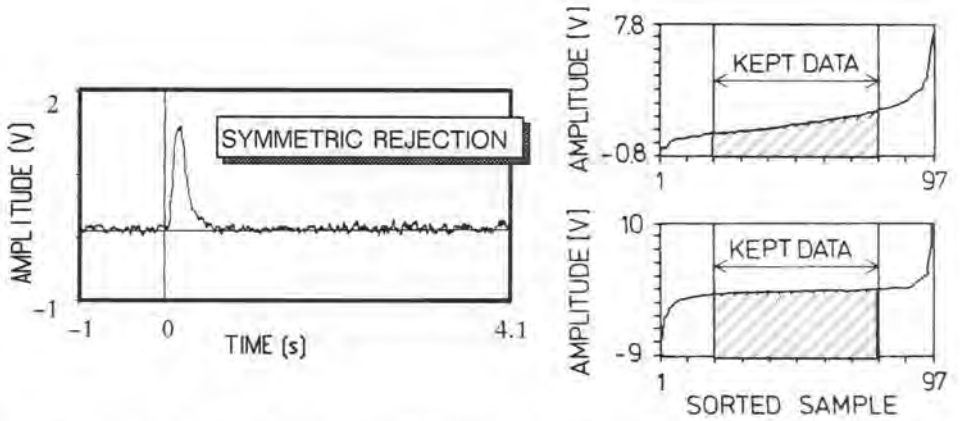

Fig. 3.10: Stacked data using the *symmetric rejection* selective stack technique with a cutoff 20% at both ends of the sorted amplitudes. The shaded areas represent the amplitudes which are all kept, all others are rejected (after Strack et al, 1989).

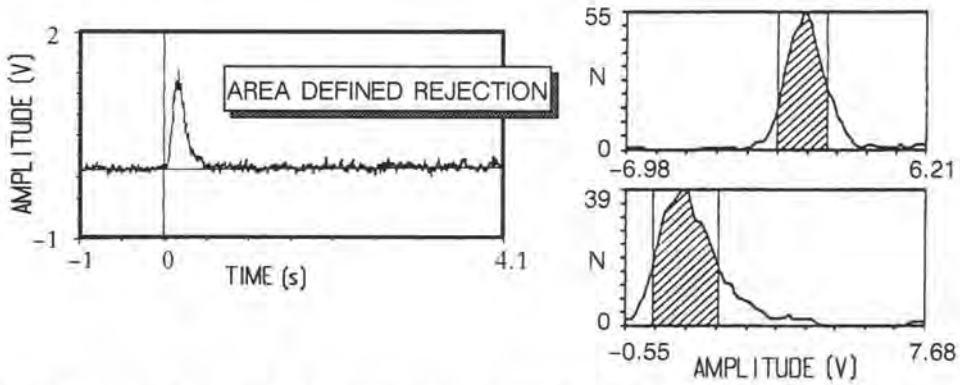

Fig. 3.11: Stacked data using the *area-defined rejection* selective stack technique with an area (shaded) defined as 60% to keep (after Strack et al, 1989).

Another more impressive example is shown in figure 3.12, where approximately 20 transients were used to derive the different stacks. The top of the figure displays the stack using a straight average of all data points without rejecting any of the high and low energy spikes. The bottom transient results from the same data set using the selective stacking algorithm with a 20% cutoff on either side of the sorted amplitude distribution. The improvement in signal-to-noise ratio is significant.

For computational speed reasons and operational ease, one can use the quartile values as rejection criteria and restrict the selection of the different stacking methods to the data sets which are still noisy after stacking.

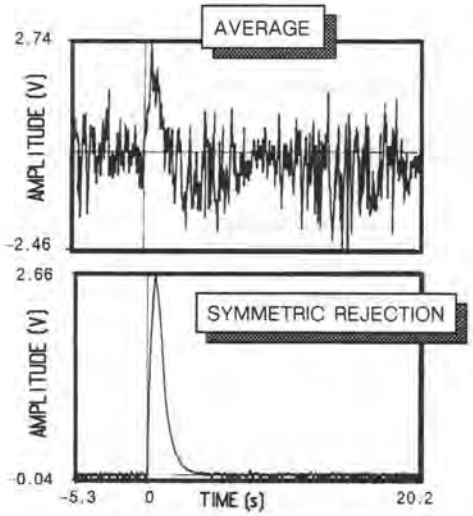

Fig. 3.12: Comparison of the selective stacking algorithm (bottom) with a straight averaging of the signal (top) using the same data (after Walker et al, 1982).

CALIBRATION FACTOR

When using controlled source electromagnetics, there are commonly two possible problems distorting the transient signal: current channeling due to lateral inhomogeneities, and incorrect amplitude measurements due to receiver misalignment and improper definition of gain, receiver area, current, A/D offsets etc. The latter becomes less important with better instrumentation and field procedures, which leaves us mainly with the effect of *static shifts* due to inhomogeneous current flow around lateral discontinuities. Unlike DC-resistivity and magnetotellurics, every interpreter finds it is difficult and often impossible to match TEM curves with *static shift* to a realistic layered earth model. This is mainly because of the stronger coupling of controlled source electromagnetic methods to the subsurface resistivity. In other words, a change in layering will not only shift the curves along the ordinate, but also distort the frequency or time scale. Vertical shifts in the apparent resistivity curves can be corrected with a correction factor which is called in this book *calibration factor*. Sometimes this factor is called *fudge factor*, or also *MMR* (magnetometric resistivity) *correction factor* (Edwards, 1978; Gomez-Trevino and Edwards, 1983) or *scale factor*, which is used as extra parameter in the inversion. It can be derived for the frequency domain from the known DC ($\omega = 0$) limit (Kaufmann and Keller, 1983; Le Roux, 1987). Stoyer applied this factor first in 1981 to transient data and subsequently it was called *calibration factor*, due to its compensation of receiver area error, which was at that time a big problem when superconducting magnetometers (SQUIDS) were used.

$$\int_0^\infty u(t)\,dt \quad \text{proportional} \quad H_z$$

and also that

$$\int_0^\infty \rho_a^{ET}\,dt \quad \text{proportional} \quad H_z$$

We now consider the integral beneath the measured voltage curve and would like to find

$$\int_0^\infty u(t)\,dt = ?$$

$$\text{where } u(t) = \frac{1}{2\pi}\int_{-\infty}^{\infty} \tilde{u}(\omega)\, e^{i\omega t}\, d\omega . \tag{3.25}$$

The time–frequency equivalents are obtained by separating Fourier transform terms into a delta function:

$$\int_{\infty}^{\infty} u(t)\,dt = \frac{1}{2\pi}\int_{-\infty}^{\infty} \tilde{u}(\omega)\,d\omega \underbrace{\int_{-\infty}^{\infty} e^{i\omega t} dt}_{2\pi\,\delta(\omega)} = \tilde{u}\,(\omega = 0) \tag{3.26}$$

$$\text{where} \int_{-\infty}^{\infty} \delta(\omega' - \omega)\, f(\omega)\, d\omega = f(\omega') \tag{3.27}$$

If we now calculate $\int_0^\infty \rho_a^{E.T.}\,dt$, we obtain:

$$\int_0^\infty \rho_a^{E.T.}\,dt = \int_0^\infty \frac{2\pi r^5}{3AD_0\,y}\, u_z(t)\,dt = \frac{2\pi r^5}{3AD_0\,y}\,\mu_0 A H_z(\omega = 0) =$$

$$= \frac{2\pi r^5}{3AD_0\,y}\,\mu_0 \frac{A D_0\,y}{4\pi r^3} = \frac{\mu_0 r^2}{6} \tag{3.28}$$

For a layered earth we obtain

$$\tilde{H}_z(\omega) = \frac{D_0\,y}{4\pi r}\left\{\frac{1}{r^2} - \int_0^\infty \frac{B_E(k) - k}{B_E(k) + k}\, J_1(kr)k\,dk\right\}. \tag{3.29}$$

For $\omega = 0$, the $B_E(\kappa) = \kappa$ is at the boundary to the bottom half-space. The recursion through the layers results in $B_E(\kappa) = \kappa$ for each layer boundary including the surface. The integrand is therefore = 0,

$$\text{or } \tilde{H}_z(\omega = 0) = \frac{D_0\ y}{4\pi}\ \frac{1}{r^3} \tag{3.30}$$

which is the same as the magnetic field of the half-space. In other words, for very low frequencies or very long recording times the electromagnetic response of a layered earth approaches the response of a half-space with the resistivity of the bottom layer.

Thus the *calibration factor* will be the same for a layered earth and the half-space. This means if we integrate the early time apparent resistivity curve, we obtain a constant which depends only on the transmitter-receiver separation and no other factors. This was first developed by Stoyer in 1981 and was subsequently tested through his students at many places around the world.

Another way of deriving the *calibration factor* is the consideration of symmetry in current flow within the subsurface (Edwards et al, 1978). Figure 3.13 illustrates this concept using a DC-monopole. The top of the figure shows a vertical section. The current flows into a conductive half-space through the monopol. Current flow is rotationally symmetric. The receiver is located at the observation site P. The bottom sketch shows a plan view of the same situation. An induction loop is located at P and the rate of change of the vertical magnetic field is measured. Each current density vector can be split into horizontal and vertical components. Only the horizontal component will yield a contribution to the vertical magnetic field in the receiver loop, because the magnetic field lines from the vertical component of the current density vector do not cross the receiver loop. The fields from the horizontal components have opposite sign and thus cancel. When using grounded wire, one can substitute it with two monopoles connected by a wire. Due to the fact that the magnetic field of a monopole is zero (rot $\mathbf{E} = 0$), at the receiver only the magnetic field from the wire connecting the two electrodes remains. This can be calculated using Biot Savart's law and the resulting value must be equal to the integral:

$$H_z^{\text{static}} = \frac{D_0}{4\pi r^2} \sin\phi = \int_0^\infty \mathring{H}_z(t)\, dt \tag{3.31}$$

Since $\mathring{H}_z$ is proportional to $\rho_a^{E.T.}$, we can now integrate the early time apparent resistivity curve and obtain:

$$\int_0^\infty \rho_a^{E.T.}\, dt = \frac{\mu_0\ r^2}{6} \tag{3.32}$$

Due to the symmetry the same derivation is true for layered earth models.

This integral allows us to define a *correction factor* or *calibration factor* as:

$$C.F. = \frac{\mu_0 \; r^2}{6 \int_0^{\infty} \rho_a^{E.T.}(t) \; dt} \tag{3.33}$$

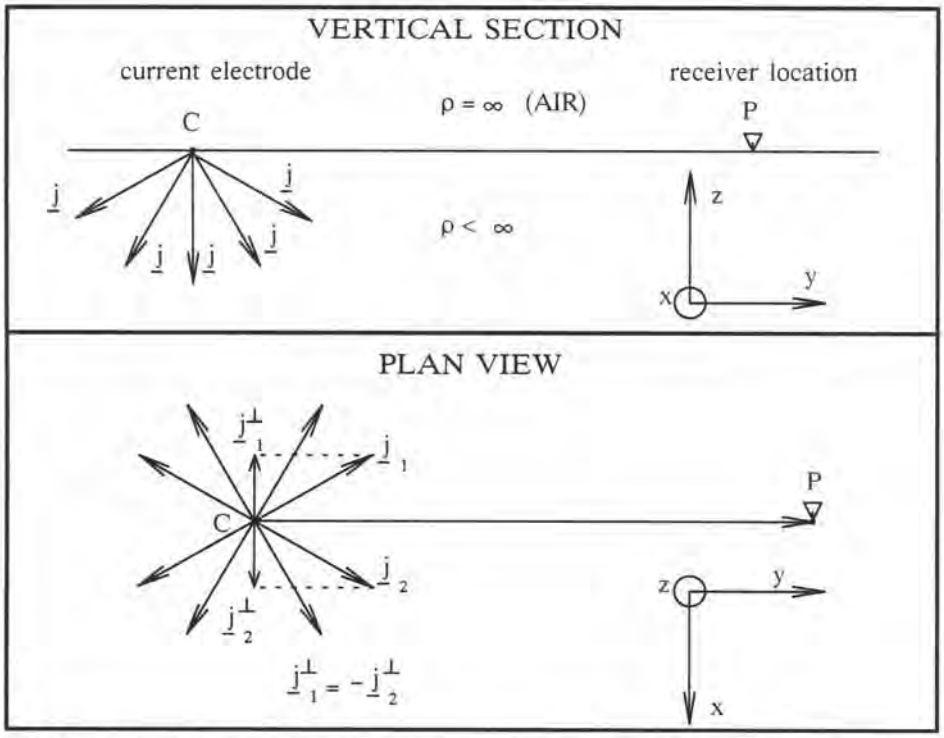

Fig. 3.13: Sketch of the symmetry within the current behavior of a DC-monopole used to visualize the effect of the calibration factor (after Hördt, 1989).

When this factor is applied it will correct the data so that the static limit is correct. We observe that for the vertical magnetic field component the above quantities only depend on the distance between transmitter and receiver. Hence the subsurface resistivity distribution has no effect on the *calibration factor*.

For real data correction the calibration factor is applied in the following manner:

- Calculate the integral with respect to time over the measured $\rho_a^{E.T.}$ curve.
- Calculate the theoretical value for that integral from the offset.
- Compare the two values and multiply the $\rho_a^{E.T.}$ curve by the ratio in case the two values do not match. This is a vertical shift of the curve on log-log coordinates.

After the above correction has been applied the distortions which manifest in vertical shifts of the apparent resistivity curve are corrected. These shifts are called *static shift* similar to seismics. Usually the word *static shift* as used in electromagnetics refers strictly to vertical parallel shifts which can be interpreted with an equivalent earth model. There may still be distortions of the transient signal through current channeling around lateral inhomogeneities in the ground which give a time dependent shift. These distortions can be called *pseudo–static* shifts which are vertical shifts for only a certain time window and the shifting factor varies between time windows. They cannot be interpreted with an equivalent model. Since this is not known before interpreting a sounding curve, the *pseudo–static* shifts are usually referred to as *static shifts*. They appear in many cases in the early time apparent resistivity curve as shifts to higher or lower resistivities leaving the impression that incorrect voltages were measured. In order to handle these shifts, an additional scale factor is provided in the inversion. Usually, one lets this factor float to compensate for minor effects caused by data editing and noise in the data.

However, if this factor is large you must be extreme care must be taken. Following is a procedure to indicate whether the *static shift* problem is present in the data set or not. At the same time it can be used to provide first order correction of the data:

- Apply the *calibration factor* to the data set. Now you are certain that any remaining shifts are not due to improper amplitude calibration.
- Use the scale factor in the inversion as a free (floating) parameter. A change required during the inversion means that the curve needs to be shifted up or down in order to obtain a satisfactory fit.
- If the *calibration factor* was changed during the inversion (larger than 20%), then this data set should be treated with great caution, because there could be some current channeling or three–dimensional effects present. For this data set it is not sufficient to rely on the validity of the first order correction which was introduced through shifting the curve. When the same behavior can be found in adjacent stations, the effect is probably caused by geologic feature. Consider this case multi–dimensional modeling.

Similar corrections may be derived for the two horizontal magnetic field components. However, their value to real data interpretation is not yet completely understood. For the electric field components, the static fields depend upon the subsurface resistivity and thus a simple *correction factor* cannot be applied. Electric field measurements are shifted in the same sense as MT data. When applying scale factors with electric fields in the inversion process, extreme care should be taken. A good way for scaling the electric field is to use an undistorted magnetic field and jointly invert the data set while keeping the scale factor for the electric field floating.

PRESTACK AND POSTSTACK PROCESSING

The above corrections build the core of a LOTEM data processing system. Most other electromagnetic systems stack the data directly at the receiver. However, we found that for deep transient electromagnetic signals, this will not work in areas with high cultural noise (Strack et al, 1989). The only way to obtain reasonable signal–to–noise ratios in those areas are prestack processing techniques. Apart from the above mentioned filter numerous simple data processing algorithms are required to correct for distortions in the signal. Table 3.1 gives a summary of most processing modules. The removal of a DC–step between the transient leader and the transient trailer should not be done prestack because the steps can only be caused by the selective stacking when the reference amplitudes are not accurately known. If this step exists in prestack data, there is a problem with the acquisition system. Notch filtering and lockin filtering should only be carried out prestack, because the periodic noise looses its line characteristics through stacking. The deconvolution of the system response can only be done prestack when the system response for the corresponding transmitter switching has been recorded. Since mostly the recorded system response is taken as average of a statistical representative number of transmitter pulses, it should usually be done poststack.

Table 3.1: Data processing modules which can be applied to LOTEM data. The X marks when this module should be applied prestack or poststack.

MODULE	PRESTACK	POSTSTACK
DC–leveling	X	X
linear drift correction	X	X
header editing	X	X
calculate amplitude spectrum	X	X
interactive data editing	X	
DC–step removal		X
pick transient onset	X	X
notch filtering	X	
lockin filtering	X	
Hanning window smoothing	X	X
time variant smoothing		X
recursive lowpass filtering	X	X
sign reversal of the data	X	
system response deconvolution		X
differentiate data	X	X
apparent resistivity transform	X	X
apply calibration factor	X	X

Figure 3.14 shows an example of prestack and poststack processing. The top frame shows a representative single transient out of 50 consecutive records recorded at a site

in central Germany. The data are strong contaminated by periodic noise. The left column shows the direct stack of the 50 records without any significant prestack processing. However, the DC-level must be removed prestack to obtain a proper reference level for the selective stacking. The stacked data set exhibits still a significant amount of noise. The data are the poststack filtered and the 16 2/3 Hz and 50 Hz periodic noise removed. Subsequently, the data are converted to apparent resistivity transforms displayed at the bottom of the figure. The right column shows the single record after applying the recursive filters for 16 2/3 Hz and 50 Hz, followed by selective stack and conversion to resistivity transforms.

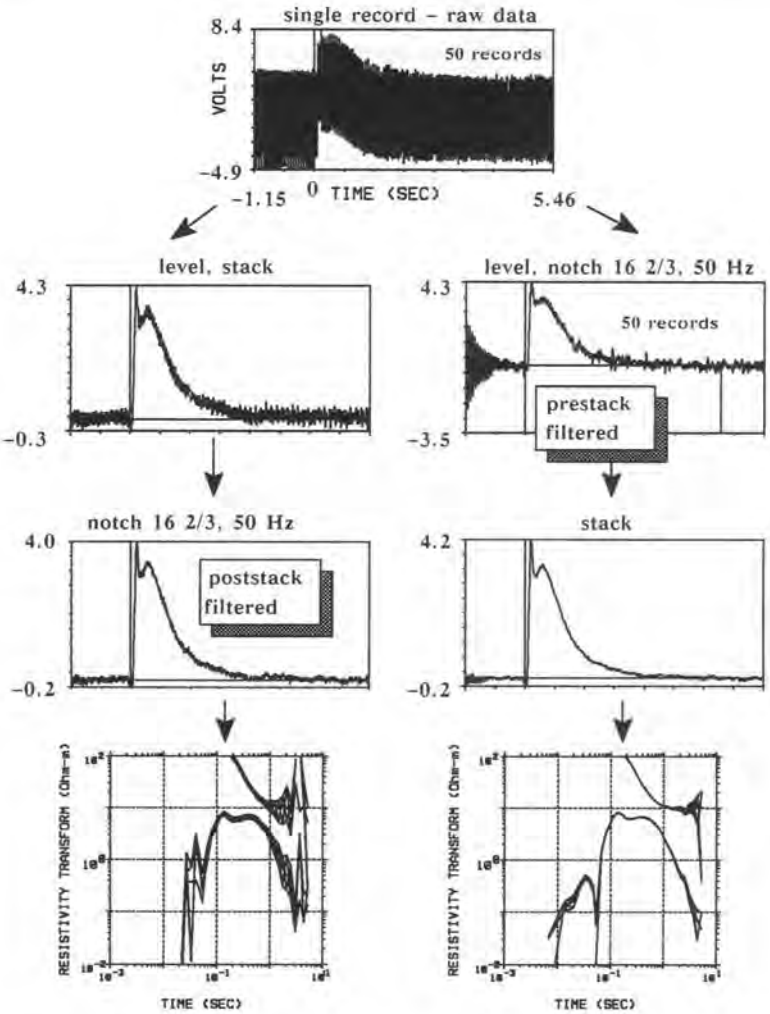

Fig. 3.14: Prestack and poststack processing example. Detailed explanation is given in the text.

After applying the digital filters poststack, some high frequency noise remains. Also, at later times in the poststack filtered data one can see some low frequency noise which is not present in the prestack filtered data (compare third row frames). The resistivity transforms of the poststack filtered data are not as smooth as the ones of the prestack filtered data. Also the error (95% confidence envelope) is significantly larger for the poststack filtered data. This is because the errors are derived from the selective stacking algorithm. A realistic error estimate is important, when one wants to use these errors as weights in the inversion. The prestack filtered data do not only appear smoother, but have also significantly smaller errors. For this example, prestack processing is the better choice to improve the signal-to-noise ratio.

SUMMARY CHAPTER 3

When recording field data, the recorded signal is influenced by systematic errors of the receiver and the transmitter as well as by sporadic errors in the instruments. The recorded signal is a convolution of the system response containing these effects with the true input signal. Thus, during data processing the system response must be accounted for in order to obtain reliable information.

The deconvolution of the system response can be done in several different ways. One way is a frequency domain deconvolution which has the disadvantage that, because of analog notch filters used in the acquisition system, it amplifies the noise and becomes unstable. Another, more stable, way is the deconvolution of the system response in the time domain which can be carried out in an iterative least squares sense. This deconvolution works well as long as the system response length is significantly shorter than the transient length and has a different frequency content.

Periodic noise caused by power lines and railroads significantly distorts the data. Since this noise is extremely strong, standard digital recursive filters – when used to remove this noise – will also distort the amplitude of the transient. However, the amplitude and shape of the signal contain essential information and must be preserved. Thus true amplitude digital recursive filters have to be used for the removal of periodic noise. True amplitude digital recursive filters can be obtained when choosing the poles and zeroes on the z-plane such that the ratio of the vectors going from the poles and zeroes to the Nyquist frequency are constant. These recursive filters remove the periodic noise without significantly distorting the transient signal.

Sporadic noise is usually caused by electric power line transients and many other effects going along with civilization. This sporadic noise usually consists of high and low energy spikes. The spikes can be eliminated by using selective stacking techniques. They are a statistical analysis of the individual data points of all recorded transients and eliminate the outliers which represent the high and low energy noise. Using this selective stacking technique a significant signal-to-noise ratio improvement can be obtained in a robust way. For different noise environments different rejection criteria for the selective stacking techniques give the optimum result.

Furthermore, the resulting signal can be distorted by current channeling near the transmitter (which is caused by small lateral inhomogeneities) or slight current channeling between the transmitter and receiver. Since the static limit of the magnetic field is independent of the resistivity of the subsurface, a characteristic scale factor for the magnetic field signal can be obtained and the resulting apparent resistivity curves can be scaled accordingly. For the electric field measurements this kind of characteristic factor cannot be derived, since the electric field dependents on the resistivity of the subsurface. In this chapter the theoretical foundation was laid for the demonstration with 3–D models and field data in the following chapter.

In areas with high cultural noise level one must apply digital processing techniques often prestack to get optimum signal–to–noise ratios. Prestack processing gives better results because the stacking process smears some of the noise characteristics, which makes the noise harder to be removed poststack.

PROBLEMS CHAPTER 3

1. The following data set is given:

RECORD:	1				
0.2755908	0.0119920	0.0000030	2.3900363	0.5832117	-0.0380386
0.1928412	0.3573927	0.1526969	0.20133	0.2706927	
RECORD:	2				
-1.5540766	-1.6780542	-1.8991159	-0.2161476	0.2473381	0.4385308
0.8813409	0.9375696	0.3787163	-0.5645440	-1.2707208	
RECORD:	3				
-1.0341588	-1.1320440	0.0740108	2.0977080	1.4319669	1.0603390
0.1261196	-0.3070775	-1.2292424	-1.3732855	-1.3503211	
RECORD:	4				
0.2017749	0.8703387	0.9356464	2.7415242	-1.2459029	-0.0844801
-1.4686812	-2.2912827	-1.3721312	-0.1848829	0.5837787	
RECORD:	5				
-2.1118524	-2.0408990	-1.3452507	2.4703624	2.9146221	2.2398403
5.0405531	-1.8007256	-1.1418511	-2.7388361	-2.8436639	
RECORD:	6				
-2.3441656	-2.5334892	-1.0664327	2.3691602	-1.0777242	-0.0351673
-1.5888555	-1.6748388	-2.0209844	-2.9484138	-0.7456929	
RECORD:	7				
-1.6146545	-0.4482726	1.0428545	3.9444280	1.5758060	-0.9646301
-1.6764526	-1.9360046	-2.6586609	-1.7716675	0.4748080	
RECORD:	8				
-2.3276727	-3.0785196	-4.3858929	-1.0590187	-0.4985634	0.6217370
-1.4811532	0.0647912	2.6683986	0.0751671	0.4168114	
RECORD:	9				
-3.1864831	-2.3261542	-1.8513770	-0.9439368	-0.9474463	-0.9302039
1.0502346	-1.8462653	-1.4414496	-2.0959754	-0.7333655	
RECORD:	10				
-1.6225488	-2.5334988	-2.2142847	0.8845467	1.1036630	1.7215295
1.6822000	0.9217781	-0.7886559	-1.9777735	0.0725502	
RECORD:	11				
1.6127090	2.2853165	1.2950211	2.4119644	-0.4884264	-1.9182514
-2.8122258	-2.0249104	-0.3581164	1.3807755	-0.8517382	

RECORD:	12				
1.8469988	2.4987781	2.3358905	3.2498157	0.4743562	-0.9259812
-0.9009567	0.0024018	1.4670550	2.0931232	2.2414386	
RECORD:	13				
-0.2569095	0.5355940	0.6386671	2.2935593	-0.2292147	-1.7735569
-2.8649800	-2.4438374	-1.4358799	-0.3457156	0.9185896	
RECORD:	14				
-0.9805466	0.5012346	2.6479175	5.4910116	3.4184101	2.1564319
-0.1822448	-1.4537216	-2.0488145	-1.5449692	0.0188661	
RECORD:	15				
-3.3838344	-3.3142543	-2.9539180	0.5495003	0.7615975	0.9481363
1.6817789	1.2588053	0.2600411	-1.3739847	-2.7665401	

Each record represents a coarsely digitized measurement (like a transient). Sequentially, each number in a record is the i-th data sample.

- Stack the above data set using the standard average. Also, calculate the standard deviation of the stack.
- Now apply the following stacking algorithm.
  - Read in the i-th sample of each record, average them and calculate the standard deviation of the read in data.
  - Sort the data points by amplitude.
  - Eliminate the outliers of the data in two possible ways
    - 20 % of all points from the lower and upper sorted data.
    - All points outside of one standard deviation.
  - Calculate from the remaining points the new average and standard deviation.
  - Read in the (i+1)-th data point of each record and repeat the above procedure.

  What is the meaning of the different stacking algorithms? Can you identify what they are being used for?

2. Derive the *calibration factor* for the horizontal magnetic field components H_x and H_y.

3. Explain in detail (mathematically) why the calibration factor for the electric field components is different from the magnetic field components.

4. Take an arbitrary early time apparent resistivity curve. Calculate the calibration factor for it. Then cut off some data points at the beginning and the end of the original curve and calculate the calibration factor. Doing this several times you can study the error introduced by editing or not editing the data.

5. Write a Fortran program to carry out deconvolution in the frequency domain. Make sure you keep the array length of the transient signal and system response variable so that you can apply it later to real data. Select a test data set (synthetic) and try out your program on the data.

6. Write a Fortran program which implements the deconvolution in the time domain. Compare the results with the results of problem 5.

KMS Technologies – KJT Enterprises Inc.
6420 Richmond Ave., Suite 610
Houston, Texas, 77057, USA
Tel: 713.532.8144

Please visit us
http://www.kmstechnologies.com